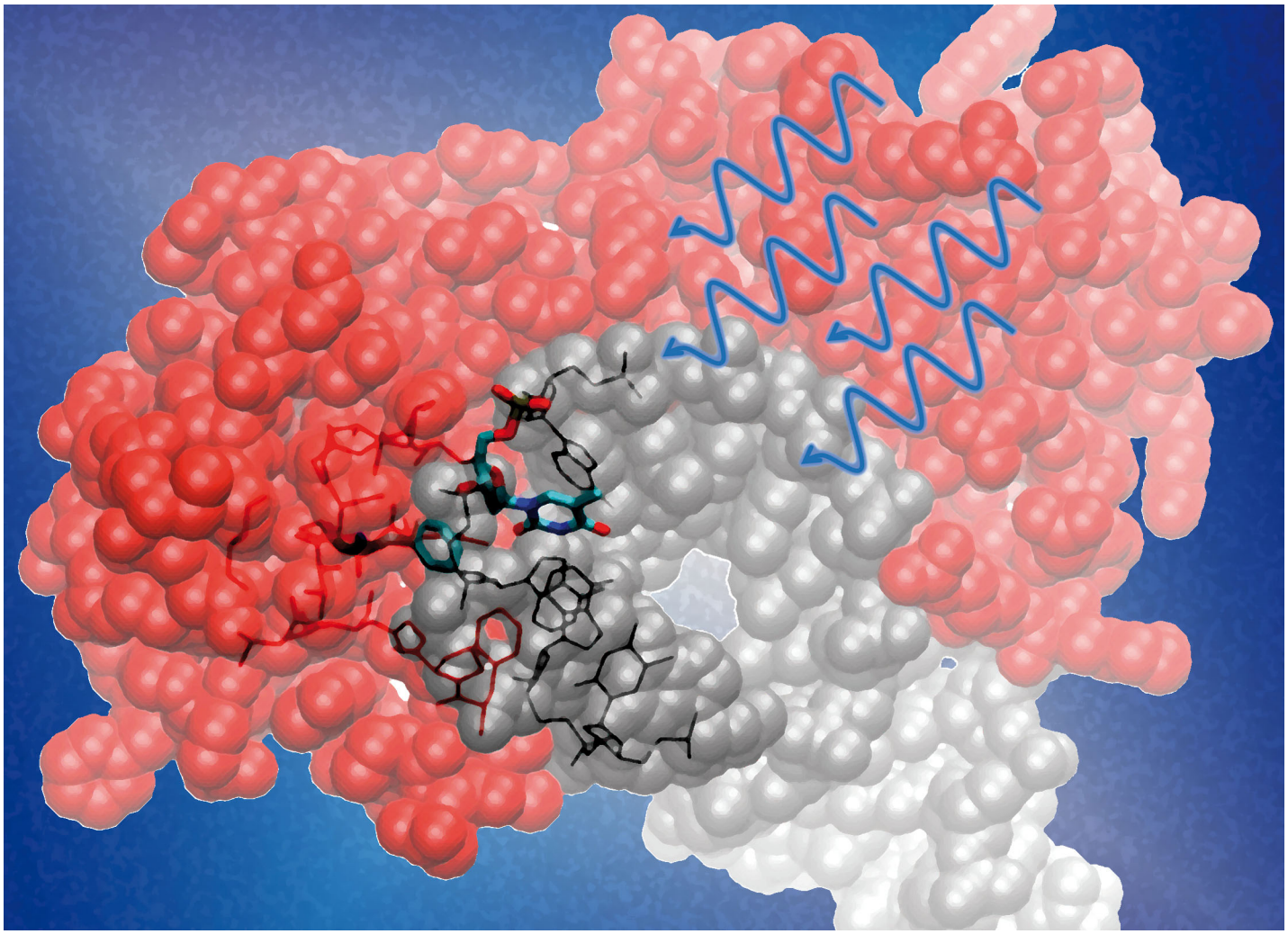

Showcasing research from the Groups of Prof. Carlo Altucci (Bio-Photonics Lab) and Dr Roberto Improta (IBB-CNR) at Federico II University, Napoli, Italy, and Prof. Majed Chergui (LSU Lab) at EPFL, Lausanne, Switzerland.

A multi-scale time-resolved study of photoactivated dynamics in 5-benzyl uracil, a model for DNA/protein interactions

Time-resolved experiments based on fluorescence up-conversion and time-correlated single photon counting reveal the excited state dynamics of biomolecules in solvents on a long time-scale from 100 fs to several ns. Modelling of these dynamics was carried out using time-dependent density functional theory, unveiling the mechanism of the ultrafast response of complicated molecules which is useful for understanding key aspects of bio-interactions such as the photoactivated dynamics of DNA/protein complexes.

As featured in:

See Majed Chergui, Roberto Improta, Carlo Altucci *et al.*, *Phys. Chem. Chem. Phys.*, 2019, **21**, 26301.

ROYAL SOCIETY OF CHEMISTRY | Celebrating IYPT 2019

rsc.li/pccp

Registered charity number: 207890

PCCP

PAPER

Cite this: *Phys. Chem. Chem. Phys.*, 2019, **21**, 26301

A multi-scale time-resolved study of photoactivated dynamics in 5-benzyl uracil, a model for DNA/protein interactions†

Mohammadhassan Valadan, [a] Enrico Pomarico,[b] Bartolomeo Della Ventura,[a] Felice Gesuele, [a] Raffaele Velotta, [a] Angela Amoresano,[c] Gabriella Pinto,[c] Majed Chergui, *[b] Roberto Improta *[d] and Carlo Altucci *[a]

Received 8th July 2019,
Accepted 14th October 2019

DOI: 10.1039/c9cp03839f

rsc.li/pccp

We combine fluorescence up-conversion and time correlated single photon counting experiments to investigate the 5-benzyl uracil excited state dynamics in methanol from 100 fs up to several ns. This molecule has been proposed as a model for DNA/protein interactions. Our results show emission bands at about 310 and 350 nm that exhibit bi-exponential sub-ps decays. Calculations, including solvent effects by a mixed discrete-continuum model, indicate that the Franck Condon region is characterized by significant coupling between the excited states of the benzyl and the uracil moieties, mirrored by the short-lived emission at 310 nm. Two main ground state recovery pathways are identified, both contributing to the 350 nm emission. The first 'photophysical' decay path involves a ππ* excited state localized on the uracil and is connected to the ground electronic state by an easily accessible crossing with S_0, accounting for the short lifetime component. Simulations indicate that a possible second pathway is characterized by exciplex formation, with partial benzene → uracil charge transfer character, that may lead instead to photocyclization. The relevance of our results is discussed in view of the photoactivated dynamics of DNA/protein complexes, with implications on their interaction mechanisms.

Introduction

The interaction between nucleic acids and several classes of proteins governs several biochemical processes: from DNA replication to protein synthesis, or cellular replication to cell apoptosis.[1–5] Much attention has been paid to the interactions of both RNA and micro-RNA with proteins of the cell nucleus, and therefore DNA, with protein partners.[6–8]

A full dynamical characterization of these interactions would surely be a fundamental step for our understanding of basic cellular processes and provide vital information for the definition of new therapeutic tools.

In this respect, time resolved (TR) optical spectroscopy techniques such as TR fluorescence resonance energy transfer[9] and fluorescence lifetime imaging microscopy experiments[10–12] have provided fundamental insights into several processes such as, for example, the encounter between ribosomal protein and RNA,[13–15] on a time-scale of a few tens of picoseconds,[16] and the sub-ps dynamical characterization of oligonucleotide–protein complexes separately performed on oligonucleotides[17–21] and proteins.[22–26]

From the experimental point of view, it is necessary to have instrumentation capable of characterizing the temporal behavior of oligonucleotide–protein complexes within a very extended time window, potentially from the sub-s down to even the sub-fs time scale.[27] In some seminal recent papers, Meech and co-workers unveiled mechanisms underlying basic functions of flavoproteins, such as phototaxis and gene regulation, by investigating the absorption response of proteins *via* transient vibrational spectroscopy over 10 decades of time (from 100 fs to 1 ms).[28] They also characterized proton transfer in fluorescent proteins *via* the green fluorescent protein technique.[29] However, a similar challenge in the case of nucleic acid (NA)/protein interactions has not yet been achieved at a molecular level to the best of our knowledge.

The inherent complexity of DNA/protein adducts makes the experimental and computational interpretation of smaller model systems extremely useful, if not mandatory. In this

[a] *Department of Physics "Ettore Pancini", University of Naples "Federico II", Naples, 80126, Italy. E-mail: carlo.altucci@unina.it*
[b] *Laboratory of Ultrafast Spectroscopy, ISIC and Lausanne Centre for Ultrafast Science (LACUS), Ecole Polytechnique Fédérale de Lausanne, CH-1015 Lausanne, Switzerland. E-mail: majed.chergui@epfl.ch*
[c] *Chemical Sciences Department, University of Naples "Federico II", Naples, 80126, Italy*
[d] *Institute for Biostructures and Bioimaging (IBB-CNR), Naples, Italy. E-mail: robimp@unina.it*

† Electronic supplementary information (ESI) available. See DOI: 10.1039/c9cp03839f

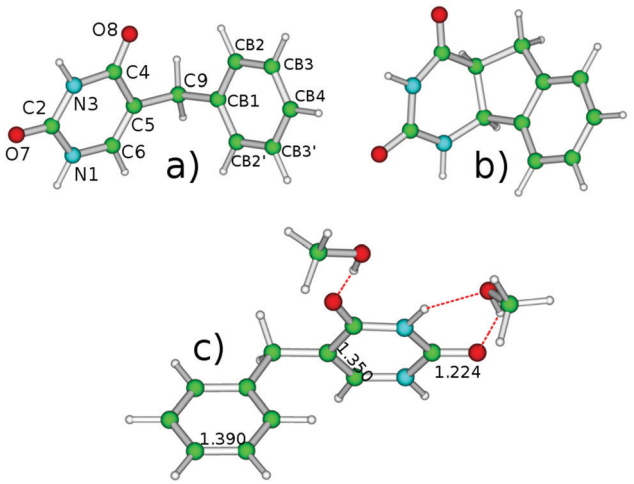

Fig. 1 Scheme of: (a) 5-benzyl uracil; (b) 5,6, benzyl uracil, formed by cyclization and H transfer reactions; (c) computational model including two methanol molecules of the 'twisted' tautomer. Atom labeling and selected bond distances in the ground state are also shown.

respect, 5-benzyl uracil (5BU Fig. 1a) is a very promising candidate. Indeed, a statistical survey of the X-ray protein structure shows that the majority of the pyrimidine bases interacting with a protein exhibit close contact (often involving ππ stacking) with the side chain of a phenylalanine (a benzene ring) or of a tyrosine (a phenol ring).[30]

Recent theoretical studies, using the multireference self-consistent field (state-averaged CASSCF) method, of the photophysics and photochemistry of a single base[31] and the steady-state optical response of 5BU[32,33] confirm the extreme interest of this system in many respects. In fact, the first and second singlet excited-states of 5BU identified possible relaxation pathways on the Potential Energy Surfaces (PESs) of the molecule, different from the pathways found for the individual moieties of uracil and benzene. Moreover, 5BU undergoes clean intramolecular photocyclization[33–35] when irradiated with UV light (≈250–260 nm), which makes it a potential model for UV-induced cross-linking reaction between thymine and phenylalanine (Fig. 1b).

Here, we study for the first time the ultrafast dynamics of 5BU, spanning a range of five decades from sub-ps to ns time scale, upon 266 nm excitation, in order to distinguish the ultrafast dynamics of the initial molecule from that of the photocyclized product. We find the appearance of a new fluorescence band in the deep UV region (310 nm) on ultrashort time scales. This completes our previous findings and fundamentally modifies the scenario of 5BU photo-dynamics with important consequences: the mechanism of 5BU ultrafast radiationless ground state recovery, analyzed by means of Time-Dependent-Density Functional Theory (TD-DFT) calculations in solution, appears to be influenced by different substitutions on the pyrimidine ring, involving the pyramidalization of C5 and the out-of-plane motion of the C5 substituent.[31,36–46]

Interestingly, the excited state dynamics of 5BU is found to be remarkably different from that of the single nucleobase references, uracil (Ura) and thymine (Thy),[38,47] due to the interaction of both bright and dark excited states of the pyrimidine moiety with a B → U Charge Transfer (CT) state. Our simulations indicate two main decay routes of excited 5BU: the photophysical pathway, a non-radiative decay to the ground state, S_0, qualitatively similar to that found in Thy, and a photochemical pathway, involving the dimerization of Ura and benzene moieties, which provides important indications on the photo-induced DNA/protein crosslinking.

Experimental and computational details

Experimental details

Experimental details are provided in the ESI.† Briefly, measurements were always performed on fresh samples and lasted no longer than 2 hours to minimize sample degradation due to photocyclization of 5BU into 5,6BU.[33] We recorded static absorption spectra before and after the measurements (see Fig. S1(a), ESI†). We also performed an additional chromatographic check, the results of which are reported in Fig. S1(b) and (c) (ESI†). We made sure that the total ion current signal of LC-MS/MS diagnostics of the targets before and after measurements remains the same. Interestingly, Fig. S1(b) (ESI†) evidences that we have only one peak before and after the experiment, confirming that no relevant change of the original chemical species took place in fluorescence up-conversion (FlUC) experiments. On the other hand, Fig. S1(c) (ESI†), where 5BU is heavily irradiated (one hundred times more than the typical dose delivered in FlUC measurements), shows an additional peak ascribed to the photocyclized species.

Nanosecond (ns)-resolved fluorescence measurements were performed using a Time Correlated Single Photon Counting (TCSPC) system described in the ESI.† Detection is performed within a window of 50 ns with an Instrument Response Function (IRF) of approximately 190 ps.

Sub-ps resolved luminescence measurements were carried out using UV FlUC,[48] also described in detail in the ESI.† Wavelength–time delay (2D) plots extended into the 280–390 nm UV region. The IRF of the FlUC system (300 fs) was determined by the temporal profile of the Raman signal of the solvent.

Computational details

As detailed in the ESI,† our calculations are based on Density Functional Theory (DFT) and TD-DFT, exploiting CAM-B3LYP[49] and M052X[50,51] functionals, and using the 6-31+G(d,p) basis set. These two long-range corrected functionals provide an accurate description of the photophysics and photochemistry of pyrimidines.[40,42–44] For what concerns the crossing region with the ground electronic state (S_0), geometry optimizations were stopped when the energy of the excited state gets too close to S_0 (energy gap < 0.3 eV), since TD-DFT calculations cannot be expected to provide an accurate description of a system in the proximity of a CI with S_0.[52,53] On the other hand, concerning the two crossing regions more relevant for this study, *i.e.* those

involved in the deactivation of the bright excited state and in the cyclization path, we have previously shown that TD/CAM-B3LYP and TD-M052X provide a description of the relevant crossing regions with S_0 very similar to that obtained by using wave function methods such as CASPT2l.[37,38,40,42–44,54,55]

Solvent effects are included by using a mixed continuum (based on the Polarizable Continuum Model, PCM)[56] discrete approach, where two methanol molecules are explicitly included in the calculations (see Fig. 1). This mixed continuum/explicit approach has already been profitably employed to study the photophysics and photochemistry of DNA.[36–38,40–42,57–59]

Results and discussion

Experimental results

A time–wavelength plot of the sub-ps fluorescence signal of 5BU in methanol between 280 and 390 nm upon excitation at 266 nm (4.66 eV) is shown in Fig. 2 (left).

The signal at 290 nm corresponds to the Raman scattering of the solvent. The emission of 5BU at early time delays is characterized by two bands centered at ≈310 and ≈350 nm, with the latter lasted longer (Fig. 2, right). In particular, both are promptly populated in time within the IRF, which is consistent with ultrafast intramolecular dynamics such as, for example, in the case of the cytosine derivatives where a single band transient absorption signal as fast as 50 fs has been reported.[64]

The kinetic traces at the band maxima are shown in Fig. 3. A bi-exponential fit convoluted with a Gaussian IRF yields the decay constants given in Table 1.

While the two τ_1 values are different, the τ_2 values are essentially identical, within error bars, suggesting that they could be attributed to the same decay mechanism.

The short component contributes relatively more to the signal at 310 nm than at 350 nm, as seen from the ratio of the pre-exponential factors: ∼3 at 310 nm, and ∼1 at 350 nm. This, in turn, is confirmed by the ratio of the signal intensity obtained from the fs and ps components, which is approximately 0.6–0.65 at 310 nm and ∼0.35 at 350 nm. Another confirmation comes from the global fit of the 2D data, showing that the spectral distribution of the amplitude associated with the second component is centered around 350 nm (see the ESI†).

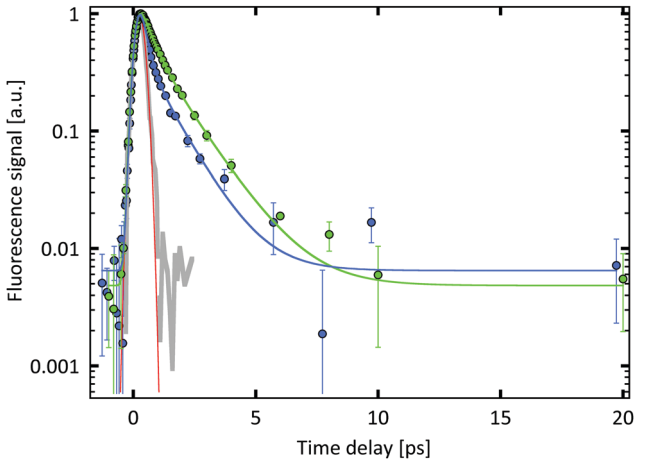

Fig. 3 Normalized kinetic traces at 310 (blue) and 350 nm (green) of the fs-resolved signal emitted by 5BU compared with the IRF of the FlUC setup. Both signals have been separately normalized to unity.

Table 1 Decay constants and their amplitudes in brackets obtained from the fit of the FlUC results

	310 nm	350 nm
τ_1	230 ± 40 fs (0.76)	440 ± 50 fs (0.53)
τ_2	1.2 ± 0.2 ps (0.24)	1.4 ± 0.1 ps (0.47)

The early time spectrum in Fig. 2 differs from the steady state spectrum (Fig. 4), due to the emission at 310 nm and its blue shifted maximum. By 3 ps, the spectrum converges to the steady-state one. Disregarding for now the feature at 310 nm, and except for the blue shift of ≈20 nm, the $t = 0$ spectrum in Fig. 4 is a near mirror image of the ground state steady-state absorption. This is commonly reported in fs fluorescence studies of various organic and inorganic molecules.[48,60,61] The ≈20 nm spectral red-shift between $t = 0$ and $t = 3$ ps can

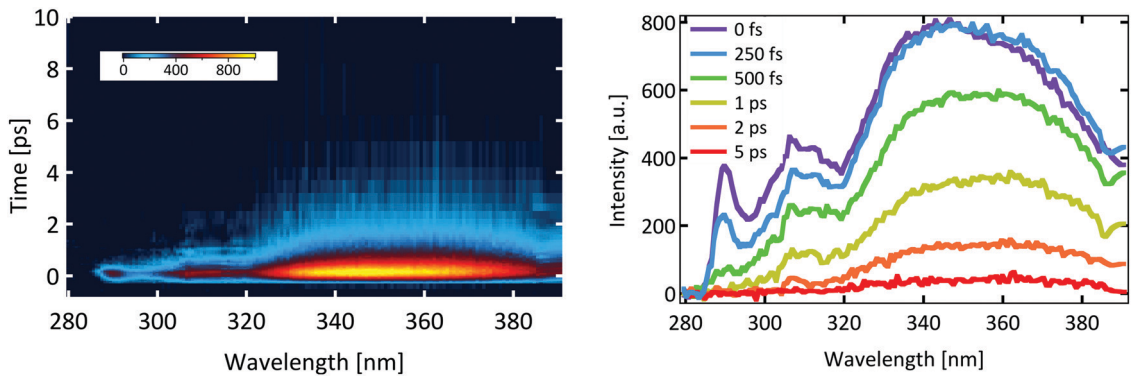

Fig. 2 (left) Time–wavelength plot of the fluorescence signal of 5BU in methanol (concentration ≈ 2.0 mM) upon excitation at 266 nm. (right) Temporal evolution of transient spectra in FlUC measurements in the sub-ps and ps range for different time-delays between pump and gate pulse in the FlUC experiment.

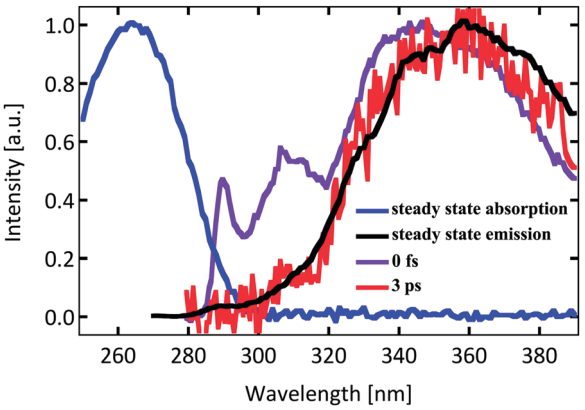

Fig. 4 Normalized spectra of 5BU in methanol upon 266 nm excitation and at time delays of 0 fs (violet) and 3 ps (red), along with the steady state spectrum (black). The steady state absorption spectrum is represented by the dark blue curve.

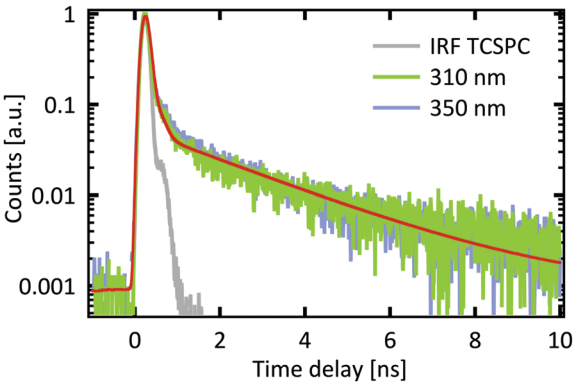

Fig. 5 Kinetic traces of the ns-resolved signal emitted by 5BU at 310 and 350 nm, in comparison with the measured IRF. A fit (red curve) of the 5BU data is also shown, obtained with a bi-exponential decay convoluted with the experimental IRF.

be due to several effects. In addition to the intramolecular effects related to the shape of the potential energy surface (PES – see the next section), it is probably due to vibrational cooling and solvent equilibration of the excited state. Dynamical solvation effects have intensely been studied in the past. It was found[62,63] that the solvent equilibration contains an inertial (Gaussian) component at early times and slower multiexponential components due to the actual solvent rearrangement. In methanol, for C153 coumarin (which exhibits an electronic transition with partial CT character), for example, a dynamical shift of *ca.* 0.3 eV was observed, and solvation dynamics has characteristic times of a few ps.[63] In our case, we observe a comparable shift occurring on a similar time-scale. Interestingly, for cytosine[64] in methanol, the fluorescence spectrum shifts by 0.12 eV within 2 ps, before reaching its 'steady state' position. These results suggest that dynamical solvent effects likely play a role in the decay of 5BU, and that the transitions involved imply an energy shift of the electron density larger than that taking place in cytosine, due to the specificity of the benzil substituent that, once excited, takes partial CT character and this changes the interaction with the methanol solvent compared to cytosine.

Fig. 5 shows the ns kinetic traces of the fluorescence signal of 5BU, measured by Time Correlated Single Photon Counting (TCSPC) at 310 and 350 nm. The kinetics are identical at both wavelengths, and the traces are fitted by a biexponential function convoluted with the IRF.[26] The fit yields a fast component in the range of $\approx$70 ps (τ^{S_1}) and a longer one of 2.4 $\pm$ 0.2 ns (τ^{S}), which corresponds to a 2% pre-exponential factor. This is a consistent contribution, in the range of $\approx$40% of the overall time-integrated signal, indicating decay with significant multi-scale character.

The above results show that the excited state decay of 5BU exhibits remarkable differences with respect to that of other pyrimidines. Besides the appearance of a ns component, the discussed 20 nm red spectral shift of the steady state emission spectrum suggests the occurrence of vibrational cooling and solvation dynamics.

However, the outstanding observation here is that a higher energy band (at $\sim$310 nm) also appears at t = 0, whose decay does not feed the lower emission band. This band is dominated by a short lived decay component (*ca.* 200 fs, Table 1 and Fig. S2, ESI†), while the 350 nm band decays in *ca.* 400 fs and 1.4 ps. For Thy, excitation at 310, 330, 350, and 370 nm did not show any clear dependence on the emission wavelength.[65] It is thus clear that the benzyl substituent leads to the appearance of new electronic states that will be analyzed in the following computational section.

Computational results

The Franck–Condon region and the absorption spectrum. The experimental results were interpreted with the help of our QM calculations. Interestingly, we find a noticeable role of the dihedral angle, θ (see Fig. 1, defined by the two planes individuated by CB2–CB1–C9 and CB1–C9–C5 atoms), in the photoactivated dynamics of 5BU, which was not highlighted in previous studies.[33,66] In fact, PCM/6-31+G(d,p) geometry optimizations predict that in the ground state (S_0) minimum, the benzene and Ura rings adopt a face-to-face arrangement (S_0 min in Table 2, see Fig. 1 and 6, with $\theta \sim 60^\circ$), enabling the maximization of $\pi\pi$ stacking interactions. On the other hand, a partially optimized minimum where the rings are constrained to an orthogonal arrangement ($\theta = 0^\circ$ in Table 2, see Fig. 1) is only 0.03 eV (*i.e.* $\sim$250 cm^{-1} and $\sim$400 cm^{-1} at the CAM-B3LYP level) less stable than the absolute minimum (see the ESI,† Table S1). Thus, the energy barrier associated with the mutual rotation of the two rings is small. Considering the sources of inaccuracy of our computational approach (density functionals and basis sets) and that only a purposely tailored dynamical study (including explicitly solute–solvent interactions and thermal effects) could provide a fully reliable quantitative description of the conformational equilibrium of 5BU, it is possible that both face-to-face and 'orthogonal' structures contribute to the photoactivated dynamics. Therefore, we performed most of our analysis for both kinds of structures in the following; if not otherwise specified, we shall mainly discuss the CAM-B3LYP results.

Table 2 Vertical excitation energy (AE in eV) of the 4 lowest energy excited states computed for 5BU·2CH_3OH in methanol solution at the PCM/TD-DFT/6-31+G(d,p) level. Oscillator strength is given in parenthesis. Notes: Thy·2CH_3OH: CAM-B3LYP: Tππ* 5.19(0.23); Tnπ* 5.46(0.00); M052X: Tππ* 5.30(0.24); Tnπ* 5.39(0.00)

		CAM-B3LYP		M052X	
	Assignment	S_0 min	$\theta = 0°$	S_0 min	$\theta = 0°$
S_1	Uππ*	5.18(0.27)	5.19(0.25)	5.20(0.20)	5.27(0.19)
S_2	Unπ/Bππ*	5.36(0.00)	5.39(0.00)	5.22(0.07)	5.34(0.07)
S_3	Bππ/Unπ*	5.43(0.00)	5.45(0.01)	5.56(0.00)	5.57(0.01)
S_4	B → U CT	5.88(0.04)	5.79(0.03)	5.89(0.04)	5.90(0.03)

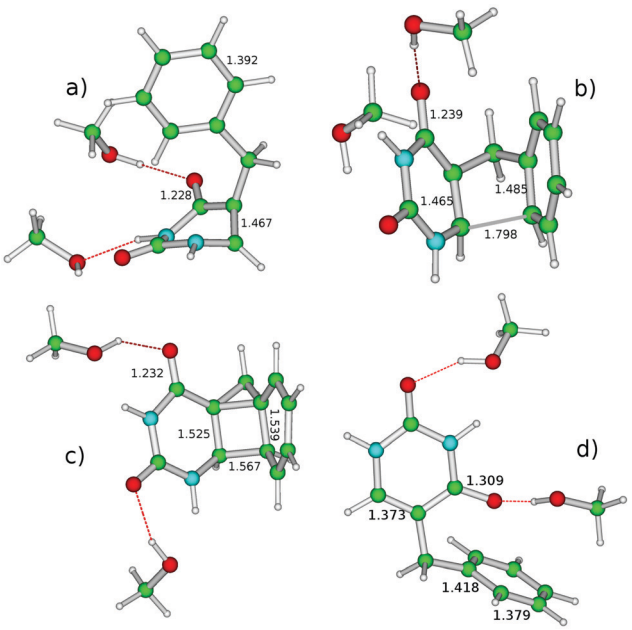

Fig. 6 Structural schematic drawing of (a) UππS_0-CI*, a representative structure of the crossing region between S_0 and the lowest energy ππ* state localized on the Ura moiety. (b) CYC-CI*, a representative structure of the crossing region between S_0 and UB-exc* state in the path leading to photocyclization (photochemical path). (c) 5BU-CYC, the photoproduct formed by photocyclization before H-transfer leads to 5,6-BU. (d) Unπ_{CT}-min color code: green for carbon, white for hydrogen, cyan for nitrogen, and red for oxygen atoms.

The computed and the experimental absorption spectra of 5BU (see Fig. S4 in the ESI†) exhibit a very similar shape. The calculated bands show a systematic blue shift (+0.5 eV). This discrepancy would be much lower (see also the ESI†) if using a larger basis set and considering thermal and vibrational effects (which are expected to lead to a systematic red-shift of −0.1–0.3 eV of the absorption maxima).[61,67] Anyway, to make the comparison with the experimental results easier, we shall also report corrected absorption (AE) and emission (EE) energies, labeled as AE_{corr} and EE_{corr} (λA_{corr} and λE_{corr} on a wavelength scale), scaled by −0.5 eV.

The four lowest energy excited states (see Table 2) derive from the interaction between three electronic transitions, two mainly related to the pyrimidine ring (Uππ* and Unπ*) and another one to the benzene moiety (hereafter Bππ*). Although the predicted spectra do not significantly depend on the relative orientation of the two rings (see columns 4 and 6 of Table 2), our calculations show that some mixing between the different transitions is always present, and it increases when the two rings are stacked.

S_1, responsible for the lowest energy absorption band around 266 nm, *i.e.* 4.66 eV, is due to an intense ππ* transition with a strong bonding/antibonding character with respect to the C5–C6 bond (see Fig. 1 for atom labeling). But, for some participation of π orbitals of benzene, S_1 is thus similar to the lowest energy bright excited state of Ura and Thy,[40–42] and we therefore label it as Uππ*.

S_2 and S_3 are mainly derived from the mixing, modulated by the orientation of the two rings, between Unπ* and Bππ*. Unπ* involves the transfer of an electron from the lone pair (LP) of the C4═O group towards a π* orbital of Ura (the LUMO), and it is thus similar to the lowest energy nπ* transition of pyrimidines. Bππ* is essentially a ππ* transition localized over the benzene ring. Finally, S_4 can be described as a B → U (CT) state.

CAMB3LYP and M052X provide a similar description of the FC region, but M052X predicts a smaller energy gap and larger coupling between Uππ*, Unπ* and Bππ*, as witnessed by the larger oscillator strength associated with S_2.

Excited state geometry optimizations

The results of the excited state geometry optimizations of S_1 strongly depend on the mutual orientation of the two rings. When optimizing the 'orthogonal' conformation, CAM-B3LYP predicts a path similar to that predicted for other substituted uracils (see the ESI† for details). A steep path leads to a flat low energy-gradient region of the PES, where the pyrimidine ring maintains a planar geometry and the main geometry shift with respect to the FC involves the increase of the C5–C6 bond distance, in line with the 'localized' nature of this excited state. In this region, the oscillator strength is rather high (0.16) and λE_{corr} = 320 nm. After this planar plateau, geometry optimization then leads directly to a non-planar minimum Uππ* (Uππ* min), where the pyrimidine ring takes a bent conformation (structure shown in Fig. S5 of the ESI†), weakly emitting with λE_{corr} ∼ 350 nm. Uππ*-min is separated by a very small energy barrier (∼0.012 eV) from a crossing region with S_0, which is reached by pyramidalization at C5, while an out-of- plane motion leads the benzene ring toward a "pseudo-perpendicular" arrangement with respect to the molecular plane (a representative structure of this region, UππS_0-CI*, is shown in Fig. 6a). At UππS_0-CI*, characterized by a C5–C6 bond distance of 1.46 Å, close to that of a CC single bond, the energy gap between Uππ* and S_0 is <0.2 eV. UππS_0-CI* is very similar to the structures of the 'ethylene-like' conical intersections involved in the non-radiative decay of the bright excited state of pyrimidines.[40,44]

When the two rings are close to a face-to-face arrangement, PCM/TD-CAM-B3LYP predicts a 'photochemical path' similar to that already described in previous works.[33,66] Geometry optimizations indicate that the partial $B^+ \rightarrow U^-$ CT character of S_1 increases, and both the pyrimidine and the benzene rings undergo a significant geometry shift and get closer

(the C6–CB2 distance decreases to 2.6 Å), until a very shallow low-gradient region (see UBexc-min, Fig. S5 in the ESI†) is reached. UBexc-min (characterized by weak emission with $\lambda E_{corr} \sim$ 350–400 nm) is not a minimum of the PES and it is 0.5 eV less stable than a close-lying crossing region with S_0. A representative structure of the crossing region, which we label as CYC-CI*, is shown in Fig. 6b. In CYC-CY*, the C5–C6 and CB2–CB3′ bond distances are significantly longer than in S_0 and, more importantly, the C6–CB2 distance is shorter than 1.8 Å, suggesting the formation of a new bond. Actually, ground state geometry optimizations starting from CYC-CI* lead, without any energy barrier, to the photoproduct shown in Fig. 6c (5BU-CYC), which is the precursor of 5,6BU, following a H-transfer reaction.[33] In the presence of only two explicit methanol molecules, this cyclization path appears extremely effective. On the other hand, as detailed in the ESI,† our new analysis suggests that solvent molecules could affect the approach between the two rings and, thus, the stability and the emission energy of UBexc-min.

Geometry optimization of the adiabatic state related to Unπ* (S_2 for the FC point and S_3 for the twisted minimum) shows an increase of the mixing with the $B^+ \rightarrow U^-$ CT state and predicts the decay to be a minimum. The analysis of the electron density (see the ESI†) shift reveals a significant B → U CT character. In the following, we shall therefore label this excited state as $Un\pi_{CT}$ and its non-emissive minimum, whose stability is similar to that of Uππ*-min and UB-exc-min, as $Un\pi_{CT}$-min. In $Un\pi_{CT}$-min, the benzene ring assumes a more quinoidal character, confirming its involvement in the transition, and the most significant geometry shift with respect to the FC point is the significant lengthening of C4–O8, as happens in the lowest energy nπ* minimum of Ura and Thy.

Geometry optimization of S_2 for the twisted structure, which has a small but non-zero oscillator strength, indicates that the system starts exploring a region of the PES where the Uππ* and the Bππ* states are strongly coupled, with a noticeable B → U CT character, similar to UBexc described above. When the rings are perpendicular, however, this state cannot proceed towards cyclization. It explores, instead, a rather flat plateau, where it is fairly emissive (an oscillator strength of 0.05–0.1) and λE_{corr} = 300–310 nm. The energy gradient in this region is rather low, but no real minimum in the PES is found and the system decays to Uππ* and, then, to its Uππ*-min.

When optimizing S_4, which has a clear B → U CT character, a similar picture is found. The strong electronic coupling between the two rings leads to the decay to Uππ*, after passing through a region characterized by emission with λE_{corr} = 300–310 nm.

M052X provides a picture of all the decay paths qualitatively similar to that obtained at the CAM-B3LYP level (see the ESI†), supporting its reliability.

A global picture of the excited state decay in 5BU

The ultrafast excited state dynamics of 5BU exhibits two main spectral components at ∼310 and ∼350 nm, both showing a bi-exponential decay. The 350 nm component dominates the FlUC spectra and the steady state fluorescence spectra.

At 310 nm, the weight of the sub-ps component is larger than that measured at 350 nm. Interestingly, radiative decay lasts a few ns to an appreciable extent, but is wavelength-independent: the dominant component at 350 nm is ∼2.4 ns, and the fluorescence at 310 nm decays with the same rate.

Only (quantum) dynamical calculations and/or direct simulation of the time-resolved spectra (well beyond the aim of the present paper) could allow a full assessment of the complex 5BU photoactivated dynamics, with four strongly interacting excited states and multiple photophysical and photochemical coupled relaxation pathways. On the other hand, on the basis of our calculations, we can propose an interpretative model (see Fig. 7), which accounts for the main experimental features and for the differences with respect to Ura and Thy.

Photophysics. We start our discussion with the emission peak at 350 nm, whose dynamics is qualitatively closer to that of the other pyrimidines, though the presence of the benzene substituent increases its complexity.

According to our model, the broad emission band extending from 300 to 500 nm is essentially related to the Uππ* state. As sketched in Fig. 7, we can distinguish the 'photophysical' pathway (in purple) and the photochemical (in red) pathway, which leads to ring closure. The orientation of the pyrimidine and the benzene moieties modulates their electronic coupling and, therefore, the interplay between these two paths.

For 'orthogonal' arrangements of the rings, the system follows a 'photophysical' path, where the excitation is mainly localized on the pyrimidine ring (Uππ* state). The minimum of Uππ* (Uππ*-min) is mainly responsible for the emission peaking at 350 nm. The Uππ* PES is very shallow and a very small energy barrier separates Uππ*-min from the crossing region with S_0. These features can explain the large spectral width of the fluorescence spectra, their small quantum yield and the very short (≈1 ps) lifetime of Uππ*. The shape of the PES, characterized by a fairly large plateau, could also explain the bi-exponential ultrafast excited state decay found, which is a common feature of pyrimidines.[40,41] It has been proposed

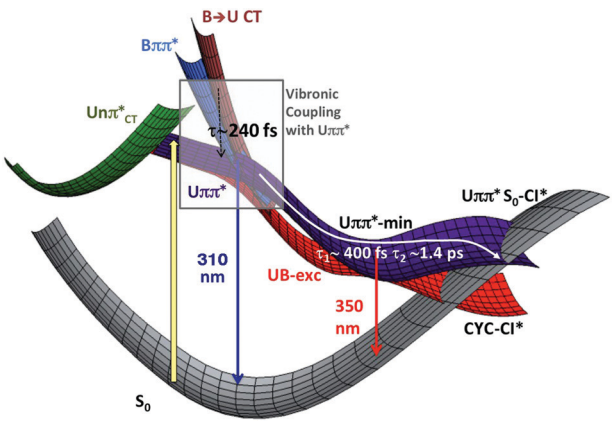

Fig. 7 Schematic drawing of the PES of the lowest energy electronic states for the 5BU molecule, with the main deactivation routes.

that the fastest constant (440 fs for 5BU) is associated with the fast motion of the WP from the FC region, through the planar plateau, towards Uππ*-min. The slowest component should instead be associated with the non-radiative decay to S_0 through the ethylene-like crossing region. On the other hand, for 5BU, other effects (such as the interaction with the other excited states) could also play a role. Furthermore, according to our calculations, the photochemical pathway is also associated with the short-lived emission at ~350 nm, further increasing the spectral width.

The decay process is accompanied by vibrational cooling, accounting for the red shift of the steady state spectrum with respect to the sub-ps peak, which is already observed after 3 ps (see Fig. 4). On balance, the photophysical path is similar to its analogue in Thy.[40,41] On the other hand, the electronic coupling with benzene is evident in this 'photophysical path', explaining the difference with respect to Ura and Thy (discussed in the following section).

Another peculiar feature of the 5BU excited state decay is the presence of a component decaying on the ns time-scale. We propose that this feature is due to a slow radiative decay associated with part of the excited population trapped within a dark excited state. Our calculations predict the existence of a very stable nπ* dark state minimum, involving the LP of the Ura moiety, with a partial $B^+ \rightarrow U^-$ CT. Only a purposely tailored quantum dynamical study could assess the Uππ* → $Un\pi_{CT}$ population transfer (and a possible back-transfer). On the other hand, the close proximity of these two states in the FC region and the stability of the $Un\pi_{CT}$ minimum suggest that a significant amount of the Uππ* population can be trapped in $Un\pi_{CT}$, in analogy with what has been proposed for Unπ in Thy and Ura.[31]

Interestingly, the involvement of dark excited states with CT character has also been proposed to explain the delayed fluorescence found in DNA.[68] Finally, 5BU-CYC could also play a role in the slow part of the dynamics, as it is more stable than CYC-CI* by only 1.7 eV and a large energy barrier can be associated with the H-transfer reaction producing 5,6BU.

Finally, we can focus on the ultrashort feature peaking at 310 nm, which represents the most outstanding feature of the ultrafast dynamics. Our calculations suggest that it is due to the electronic coupling between the two rings. As shown in Table 2, the two lowest energy excited states of the pyrimidine moiety (Uππ* and Unπ*) and the lowest excited states of B (Bππ*) fall close in energy in the FC region and are electronically coupled, as shown by their non-zero oscillator strength (see Table 2). Interestingly, the coupling is observed both for orthogonal and face-to-face arrangements. Actually, also for orthogonal structures, where the benzene and uracil π-orbitals interact less, the oxygen LP provides an additional source of coupling between the two rings. In other words, in the FC region, we have four electronic transitions, one bright and three less intense, but all of them can be populated by excitation at 266 nm. Our excited state geometry optimizations indicate that the excited states more related to Bππ* reach a region where the coupling with the bright Uππ* state increases. This region is characterized by emission at ~310 nm, and, since the Uππ* state mostly contributes also to the emission at ~350 nm, we can infer an upper limit of ~300 fs (the IRF) for the time it takes for Uππ* to reach this region. On the other hand, no real minimum is present on their PES, they are strongly coupled with the underlying Uππ* and Unπ* and the density of states in the FC region is high. These factors explain why the 310 nm peak disappears within a few hundreds of fs, decaying to the lower-lying excited states. It is not possible, without a proper inclusion of vibronic coupling, to be sure about the final fate of this '310' population. Our optimizations suggest the decay to Uππ*, *i.e.* increasing the photoexcited population already evolving in this state. This picture would be consistent with the strong similarity of the 'slow' (>1 ps) components of the decay at 310 and 350 nm. In other words, after the vibronic cascade to the lower Uππ* state is completed in a few hundreds of fs, all the WP evolves in this latter state (which also emits at 310 nm). On the other hand, decay to the $Un\pi_{CT}$ dark state is also possible, accounting for the 'sudden' disappearance of the fluorescence signal. In this scenario, in 5BU, it would be possible to observe the population of the dark excited state, which in the other pyrimidines is masked by the blue-shift of the main fluorescence band.

Photochemistry. The photochemical pathway is associated with the UB exciplex (with a partial $B^+ \rightarrow U^-$ CT character), confirming previous analysis. Our new calculations enable appreciating the importance of the mutual orientation of the ring, which modulates the interplay between photophysical and photochemical pathways. The UB exciplex is indeed populated only for the face-to-face arrangement of the two rings, then leading to 5BU-CYC, the precursor of 5,6BU. This 'photochemical' path is almost barrierless, accounting for the fairly high photocyclization yield (10^{-3}).[33,34] On the other hand, an additional reaction step is necessary to reach the final photoproduct and only the partially stacked conformation is photochemically active, decreasing the 5,6BU quantum yield. This provides useful hints on the kind of coordination geometry that would allow photodimerization in the case of NA/protein adducts. Furthermore, according to our computations, the photocyclization yield could depend on the solvent: a more polar solvent will favor stacked conformations thereby decreasing the solvent exposed surface and, hence, increasing the photocyclization yield. In contrast, less polar solvents leading to less stacked minima and high solute/solvent dispersion interaction, would have the opposite effect. The presence of the solvation cage around the rings can thus reduce the cyclization yield, which could be sensitive to changes in the solvent, or, in the case of NA/protein complexes, to the local polarity of the medium.

Since, according to our analysis, both photochemical and photophysical pathways are characterized by the short-lived emission at ~350 nm, it does not seem possible to discriminate them by fluorescence. As it happens for Thy/Thy dimerization,[69] other techniques, *e.g.* time resolved IR spectroscopy, could be informative.

Substituent effect on the excited state decay of pyrimidine

A critical comparison between the results obtained for 5BU and those available for Thy and Ura provides interesting insights on

the effect of the substituent in the photoactivated dynamics of pyrimidine bases. For 5BU, we found a bi-exponential decay with two components with similar weight τ_1 = 440 fs and τ_2 = 1.4 ps. For Thy, time resolved experiments in hydrogen bonding solvents show instead a bi-exponential decay, with a fast component of $\sim$100 fs and slower one of $\sim$500 fs, resulting in a τ average, $\langle\tau\rangle$, between 200 and 540 fs depending on the adopted technique.[37,70–72] For Ura, the ground state recovery occurs on a $<$100 fs time-scale.[38]

Our data show that the presence of the benzene substituent notably slows down the kinetics of Ura, more than a simple methyl substituent, confirming the sensitivity of pyrimidine photophysics to the nature of the C5 substituent. The crossing region between Uππ* and S_0 is reached by pyramidalization at the C5 substituent and out of plane motion of the C5 substituent. Substituents that, for hyperconjugative and/or inductive effects, stabilize sp^2 hybridization at C5 increase the energetic cost of this rearrangement (which is barrierless in Ura) and stabilize Uππ*-min. In 5BU, the C5–C9 bond distance decreases by more than 0.02 Å when going from the FC region to Uππ*-min and this shift is accompanied by small changes in the CC distance of the benzene moiety. The longer excited state lifetime of Uππ* in 5BU is due not only to the steric hindrance of the benzene substituent, but also to the onset of electronic interactions between the π systems of the benzene and pyrimidine moieties.

The presence of the benzene moiety also affects the main features of the dark Unπ*, the other excited state that, in addition to Uππ*, could be involved in the photophysics of pyrimidine following excitation in the UV region. For 5BU, Unπ is mixed with the B → U CT state, in the FC region and even more at its minimum. As a consequence: (i) the energy gap between Uππ and Unπ_{CT} in the FC region slightly decreases with respect to what is found in Thy, increasing the possibility that this state is populated by laser excitation; (ii) the structure of the minimum changes; (iii) the energy gap with respect to the crossing region with Uππ increases.

Conclusions

In this study, we reported photoactivated dynamics of 5BU obtained by TR fluorescence experiments, on time scales ranging from 100 fs to some ns. The results of the experiments are interpreted with the help of QM calculations with implicit solvent. Ultrafast radiative decay of 5BU has components in all the investigated regimes: fs, ps, and ns. Only one long-lived wavelength-independent slow lifetime (τ^S = 2.4 ns) is found, whereas the ultrafast dynamics is complex, with two different features, characterized by emission maxima at 310 and 350 nm, both with a bi-exponential decay in the sub-ps and ps regimes. The 350 nm component, corresponding to the maximum of the steady state fluorescence peak, can be ascribed mainly to a minimum in the main 'photophysical' pathway, similar to the main decay route in pyrimidine (Uππ* state). It is characterized by bi-exponential decay with τ_1 = 440 fs and τ_2 = 1.4 ps. In addition, simulations suggest that the photochemical pathways, active for the face-to-face stacking arrangement of the two rings, can contribute to 350 nm emission.

The emission at 310 nm, which is a novel feature, is instead characterized by a relevant component having a shorter lifetime, τ_1 = 230 fs, with a longer decay component, τ_2 = 1.4 ps. The former is likely due to the decay from the excited states to Uππ*, by acquiring oscillator strength thanks to the vibronic coupling with the spectroscopic state.

According to our calculations, the photo-dynamics of 5BU is governed by the electronic coupling between the pyrimidine and the benzene rings. B → U CT states, bright and dark pyrimidine excited states, are close in energy and can modulate the photophysics of the system, opening up exciting possibilities for the study of NA/protein interactions. For example, the 310 nm signature could be, in principle, a flag of NA/protein interactions. Furthermore, the involvement of an electronic transition with peculiar properties as B → U CT could be used to study NA/polypeptide interactions, especially considering the presence of components decaying on the ns time-scale. This CT transition is indeed potentially sensitive to variation of different parameters that can work as probes of the base/peptide interactions, such as relative orientation of the rings, local polarity and electric field of the embedding medium, and ionic strength.

We also provide the first 'indirect' TR indication on the cross-linking interaction between the pyrimidine and the benzene ring. Our results are consistent with a fast formation of the photoadduct ($\leq$3 ps), in analogy to what was found for cyclobutane pyrimidine dimer formation in DNA.[20]

Applications rely on the possibility to monitor the novel UV band emission by the target under study, which is only due to relaxation of the excited 5BU molecule to its ground state with no photocyclization. This can be done either by just filtering the emitted spectrum to isolate the UV component, or by also time-gating the emitted fluorescence to reach a better signal-to-noise ratio getting rid of eventual spurious emission in the same spectral window by long lived impurities.

Conflicts of interest

There are no conflicts to declare.

Acknowledgements

We acknowledge the Swiss NSF *via* the NCCR:MUST for support. The authors thank Dr Lara Martinez Fernandez for useful discussions. R. I. thanks CNR, Progetto Bilaterale CNR/CNRS PICS 2015 and the Université Paris-Saclay (Programme D'Alembert). M. V., R. V., and C. A. thank Dr Marco Micciarelli for fruitful discussions.

References

1 K. J. Durniak, S. Bailey and T. A. Steitz, *Science*, 2008, **322**(5901), 553–557.

2 T. A. Steitz, *Nat. Rev. Mol. Cell Biol.*, 2008, **9**(3), 242–253.
3 M. Selmer, C. M. Dunham, F. V. Murphy IV, A. Weixlbaumer, S. Petry, A. C. Kelley, J. R. Weir and V. Ramakrishnan, *Science*, 2006, **313**(5795), 1935–1942.
4 V. Ramakrishnan, *Cell*, 2014, **159**(5), 979–984.
5 R. Berisio, F. Schluenzen, J. Harms, A. Bashan, T. Auerbach, D. Baram and A. Yonath, *Nat. Struct. Biol.*, 2003, **10**(5), 366–370.
6 J. D. Buenrostro, C. L. Araya, L. M. Chircus, C. J. Layton, H. Y. Chang, M. P. Snyder and W. J. Greenleaf, *Nat. Biotechnol.*, 2014, **32**(6), 562–568.
7 P. H. Higgs and N. Lehaman, *Nat. Rev. Genet.*, 2015, **16**(1), 7–17.
8 S. A. Mortimer, M. A. Kidwell and J. A. Doudna, *Nat. Rev. Gent.*, 2014, **15**(7), 469–479.
9 T. Förster, *Ann. Phys.*, 1948, **6**, 55–75.
10 A. Esposito, H. C. Gerritsen and F. Wouters, *Biophys. J.*, 2005, **89**(6), 4286–4299.
11 M. A. Digma, V. R. Caiolfa, M. Zamai and E. Gratton, *Biophys. J.*, 2008, **94**(2), L14–L16.
12 R. Yasuda, C. D. Harvey, H. N. Zhong, A. Sobczyk, L. van Aelst and K. Svoboda, *Nat. Neurosci.*, 2006, **9**(2), 283–291.
13 H. Kim, S. C. Abeysirigunawarden, K. Chen, M. Mayerle, K. Ragunathan, Z. Luthey-Schulten, T. Ha and S. A. Woodson, *Nature*, 2014, **506**(7488), 334–338.
14 S. C. Abeysirigunawardena, H. Kim, J. Lai, K. Ragunathan, M. C. Rappe, Z. Luthey-Schulten, T. Ha and S. A. Woodson, *Nat. Commun.*, 2017, **8**, 492.
15 S. Blouin, T. D. Craggs, D. A. Lafontaine and J. C. Penedo, *Methods Mol. Biol.*, 2009, **543**, 475–502.
16 S. Padilla-Parra, N. Audugé, M. Coppey-Moisan and M. Tramier, *Biophys. J.*, 2008, **95**(5), 2976–2988.
17 C. T. Middleton, K. de La Harpe, C. Su, Y. K. Law, C. E. Crespo-Hernández and B. Kohler, *Annu. Rev. Phys. Chem.*, 2009, **60**, 217–239.
18 J. M. L. Pecourt, J. Peon and B. Kohler, *J. Am. Chem. Soc.*, 2000, **122**(38), 9348–9349.
19 C. E. Crespo-Hernández, B. Cohen and B. Kohler, *Nature*, 2005, **436**(7054), 1141–1144.
20 W. J. Schreier, T. E. Schrader, F. O. Koller, P. Clich, C. E. Crespo-Hernández, V. N. Swaminathan, T. Carell, W. Zinth and B. Kohler, *Science*, 2007, **315**(5812), 625–629.
21 F. Santoro, V. Barone and R. Improta, *Proc. Natl. Acad. Sci. U. S. A.*, 2007, **104**(24), 9931–9936.
22 S. K. Pal, L. Zhao and A. H. Zewail, *Proc. Natl. Acad. Sci. U. S. A.*, 2003, **100**(24), 8113–8118.
23 M. Kondo, I. A. Heisler, D. Stoner-Ma, P. J. Tonge and S. R. Meech, *J. Am. Chem. Soc.*, 2010, **132**(5), 1452–1453.
24 D. Polli, P. Altoè, O. Weingart, K. M. Spillane, C. Manzoni, D. Brida, G. Tomasello, G. Orlandi, P. Kukura, R. A. Mathies, M. Garavelli and G. Cerullo, *Nature*, 2010, **467**(7314), 440–443.
25 R. Monni, A. Al Haddad, F. Van Mourik, G. Aubock and M. Chergui, *Proc. Natl. Acad. Sci. U. S. A.*, 2015, **112**(18), 5602–5606.
26 J. Leonard, E. Portuondo-Campa, A. Cannizzo, F. van Mourik, G. van der Zwan, J. Tittor, S. Haacke and M. Chergui, *Proc. Natl. Acad. Sci. U. S. A.*, 2009, **106**(19), 7718–7723.
27 F. Calegari, D. Ayuso, A. Trabattoni, L. Belshaw, S. De Camillis, S. Anumula, F. Frassetto, L. Poletto, A. Palacios, P. Decleva, J. B. Greenwood, F. Martin and M. Nisoli, *Science*, 2014, **346**(6207), 336–339.
28 R. Brust, A. Lukacs, A. Haigney, K. Addison, A. Gil, M. Towrie, I. P. Clark, G. M. Greetham, P. J. Tonge and S. R. Meech, *J. Am. Chem. Soc.*, 2013, **135**(43), 16168–16174.
29 S. R. Meech, *Chem. Soc. Rev.*, 2009, **38**(10), 2922–2934.
30 S. Usha and S. Selvaraj, *J. Biomol. Struct. Dyn.*, 2014, **32**(10), 1686–1704.
31 R. Improta, V. Barone, A. Lami and F. Santoro, *J. Phys. Chem. B*, 2009, **113**(43), 14491–14503.
32 M. Micciarelli, C. Altucci, B. Della Ventura, R. Velotta, V. Toşa, A. B. Gónzalez Pérez, M. Pérez Rodríguez, Á. R. de Lera and A. Bende, *Phys. Chem. Chem. Phys.*, 2013, **15**(19), 7161–7173.
33 M. Micciarelli, M. Valadan, B. Della Ventura, G. Di Fabio, L. De Napoli, S. Bonella, U. Röthlisberger, I. Tavernelli, C. Altucci and R. Velotta, *J. Phys. Chem. B*, 2014, **118**(19), 4983–4992.
34 G. Sun, C. Fecko, R. Nicewonger, W. Webb and T. Begley, *Org. Lett.*, 2006, **8**(4), 681–683.
35 C. J. Fecko, K. M. Munson, A. Saunders, G. Sun, T. P. Begley, J. T. Lis and W. W. Webb, *Photochem. Photobiol. Sci.*, 2007, **83**(6), 1394–1404.
36 Á. Bányász, S. Karpati, Y. Mercier, M. Reguero, T. Gustavsson, D. Markovitsi and R. Improta, *J. Phys. Chem. B*, 2010, **114**(39), 12708–12719.
37 F. Santoro, V. Barone, T. Gustavsson and R. Improta, *J. Am. Chem. Soc.*, 2006, **128**(50), 16312–16322.
38 T. Gustavsson, Á. Bányász, E. Lazzarotto, D. Markovitsi, G. Scalmani, M. J. Frisch, V. Barone and R. Improta, *J. Am. Chem. Soc.*, 2006, **128**(2), 607–619.
39 S. Yamazaki and T. Taketsugu, *J. Phys. Chem. A*, 2012, **116**(1), 491–503.
40 R. Improta, F. Santoro and L. Blancafort, *Chem. Rev.*, 2016, **116**(6), 3540–3593.
41 M. Barbatti, A. C. Borin and S. Ullrich, Topics in Current Chemistry, Photoinduced Phenomena in Nucleic Acids I: Nucleobases in the Gas Phase and in Solvents, 2015, vol. 355, especially chapters: Excitation of Nucleobases from a Computational Perspective I: Reaction Paths; A. Giussani, J. Segarra-Martí, D. Roca-Sanjuán and M. Merchán, pp. 57–97; Excitation of Nucleobases from a Computational Perspective II: Dynamics S. Mai, M. Richter, P. Marquetand and L. González, pp. 99–153.
42 R. Improta and V. Barone, *Top. Curr. Chem.*, 2015, **355**, 329–357.
43 A. J. Pepino, J. Segarra-Martí, A. Nenov, I. Rivalta, R. Improta and M. Garavelli, *Phys. Chem. Chem. Phys.*, 2018, **20**(10), 6877–6890.
44 A. J. Pepino, J. Segarra-Martí, A. Nenov, R. Improta and M. Garavelli, *J. Phys. Chem. Lett.*, 2017, **8**(8), 1777–1783.
45 S. Matsika, *J. Phys. Chem. A*, 2004, **108**(37), 7584–7590.
46 D. Keefer, S. Thallmair, S. Matsika and R. de Vivie-Riedle, *J. Am. Chem. Soc.*, 2017, **139**(14), 5061–5066.
47 B. M. Pilles, B. Maerz, J. Chen, D. B. Bucher, P. Gilch, B. Kohler, W. Zinth, B. P. Fingerhut and W. J. Schreier, *J. Phys. Chem. A*, 2018, **122**(21), 4819–4828.

48 A. Cannizzo, O. Bram, G. Zgrablic, A. Tortschanoff, A. A. Oskouei, F. van Mourik and M. Chergui, *Opt. Lett.*, 2007, **32**(24), 3555–3557.
49 Y. Zhang, J. Dood, A. Beckstead, X. Li, K. Nguyen, C. Burrows, R. Improta and B. Kohler, *Proc. Natl. Acad. Sci. U. S. A.*, 2014, **111**(32), 11612–11617.
50 Y. Zhao, N. E. Schultz and D. G. Truhlar, *J. Chem. Theory Comput.*, 2006, **2**(2), 364–382.
51 Y. Zhao and D. G. Truhlar, *Acc. Chem. Res.*, 2008, **41**(2), 157–167.
52 B. G. Levine, C. Ko, J. Quenneville and T. Martinez, *J. Mol. Phys.*, 2006, **104**, 1039.
53 L. Gonzales, D. Escudero and L. Serrano-Andres, *ChemPhysChem*, 2012, **13**, 28–51.
54 R. Improta, *J. Phys. Chem. B*, 2012, **116**(49), 14261–14274.
55 I. Conti, L. Martínez-Fernández, L. Esposito, S. Hofinger, A. Nenov, M. Garavelli and R. Improta, *Chem. – Eur. J.*, 2017, **23**(60), 15177–15188.
56 J. Tomasi, B. Mennucci and R. Cammi, *Chem. Rev.*, 2005, **105**(8), 2999–3093.
57 L. Esposito, A. Banyasz, T. Douki, M. Perron, D. Markovitsi and R. Improta, *J. Am. Chem. Soc.*, 2014, **136**(31), 10838–10841.
58 A. Banyasz, T. Douki, R. Improta, T. Gustavsson, D. Onidas, I. Vayá, M. Perron and D. Markovitsi, *J. Am. Chem. Soc.*, 2012, **134**(36), 14834–14845.
59 A. Banyasz, L. Martinez-fernandez, T. M. Ketola, A. Munoz-losa, L. Esposito, D. Markovitsi and R. Improta, *J. Phys. Chem. Lett.*, 2016, **7**(11), 2020–2023.
60 O. Bräm, F. Messina, A. M. El-Zohry, A. Cannizzo and M. Chergui, *Chem. Phys.*, 2012, **393**(1), 51–57.
61 O. Bräm, T. J. Penfold, A. Cannizzo and M. Chergui, *Phys. Chem. Chem. Phys.*, 2012, **14**(10), 3513–3519.
62 R. Jimenez, G. R. Fleming, P. V. Kumar and M. Maroncelli, *Nature*, 1994, **369**, 471–473.
63 M. L. Horng, J. A. Gardecki, A. Papazyan and M. Maroncelli, *J. Phys. Chem.*, 1995, **99**(48), 17311–17337.
64 C. Ma, C. C. Cheng, C. T. Chan, R. C. Chan and W. Kwok, *Phys. Chem. Chem. Phys.*, 2015, **17**(29), 19045–19057.
65 D. Onidas, D. Markovitsi, S. Marguet, A. Sharonov and T. Gustavsson, *J. Phys. Chem. B*, 2002, **106**(43), 11367–11374.
66 M. Micciarelli, B. F. E. Curchod, S. Bonella, C. Altucci, M. Valadan, U. Rothlisberger and I. Tavernelli, *J. Phys. Chem. A*, 2017, **121**(20), 3909–3917.
67 F. J. Avila Ferrer, J. Cerezo, E. Stendardo, R. Improta and F. Santoro, *J. Chem. Theory Comput.*, 2013, **9**(4), 2072–2082.
68 I. Vayá, T. Gustavsson, T. Douki, Y. Berlin and D. Markovitsi, *J. Am. Chem. Soc.*, 2012, **134**(28), 11366–11368.
69 S. Marguet and D. Markovitsi, *J. Am. Chem. Soc.*, 2005, **127**(16), 5780–5781.
70 T. Gustavsson, Á. Bányász, N. Sarkar, D. Markovitsi and R. Improta, *Chem. Phys.*, 2008, **350**, 186–192.
71 F. Buchner, A. Nakayama, S. Yamazaki, H. Ritze and A. Lübcke, *J. Am. Chem. Soc.*, 2015, **137**(8), 2931–2938.
72 J. M. L. Pecourt, J. Peon and B. Kohler, *J. Am. Chem. Soc.*, 2001, **123**(42), 10370–10378.

